IEEE Access
Multidisciplinary ⋮ Rapid Review ⋮ Open Access Journal

Received 29 January 2024, accepted 8 February 2024, date of publication 22 February 2024, date of current version 1 March 2024.

Digital Object Identifier 10.1109/ACCESS.2024.3368883

RESEARCH ARTICLE

High-Performance Extrinsic Fabry-Perot Fiber Optic Acoustic Sensor Based on Au/PI Composite Film

ZEKUN ZHU, HANYU SHUAI, KUN JIA, YUANYUAN SUN, BO JIA, AND PENGWEI ZHOU
Department of Materials Science, Fudan University, Shanghai 200433, China

Corresponding author: Pengwei Zhou (pwzhou@fudan.edu.cn)

This work was supported by the Science and Technology Commission of Shanghai Municipality under Grant 17DZ2280600.

ABSTRACT This paper reports a novel Fabry-Perot fiber optic microphone based on Au/PI composite film, with an optimal F-P cavity length of 500 μm, and the maximum extinction ratio (ER) obtained is about 12 dB. Besides, the sensor has flat response performance in the audio frequency range of 200-10 kHz, with a maximum signal-to-noise ratio (SNR) of 76 dB and a sensitivity of approximately 170 mV/Pa at the sound pressure level of 1000 Hz/94 dB, which is much higher than Brüel & Kjær's electric microphone 4939. Within a certain range of sound pressure, there is a fine linear relationship between the output response of the sensor and the input sound pressure, with a fitting coefficient of 0.9987. The new diaphragm-type fiber optic microphone proposed in our work has superb economy, sensitivity, frequency response and linearity within the audible sound range, which is expected to achieve large-scale, low-cost fabrication and long-term stable application in audio detection and other fields.

INDEX TERMS Optical fiber sensors, Fabry-Perot cavity, acoustic measurements.

I. INTRODUCTION

In the modern era of rapid development of information technology, sound waves, as a carrier of information and energy, have received widespread attention from researchers. Realizing accurate detection of sound signals has vital academic value and strategic significance. In previous work, research on sound signals was typically carried out using electroacoustic technology. Recently, with breakthroughs in the field of fiber optic sensing, the research hotspot of acoustic sensors has shifted from electroacoustic sensing technology to photoacoustic sensing technology as well. Compared with electroacoustic sensors, photoacoustic sensors have advantages such as high sensitivity and resistance to electromagnetic interference.

While some fiber optic acoustic sensors are designed to detect infrasound/ultrasound, they are still of academic interest and practical value for detection in the audible acoustic range (20-20 kHz). In addition to the literature that have been reported [1], [2], [3], mature products have emerged on the market, such as Optimic 1140, an optical fiber microphone launched by Optoacoustics, Israel, which is used for indoor acoustic monitoring and other applications. In addition, photoacoustic sensors for detecting audible sound bands have huge potential in various scenarios such as MRI/MEG scanning, high-voltage equipment maintenance, aerospace measurement, and so on [4].

According to different modulated optical parameters, fiber optic acoustic sensors could be classified into intensity type, phase type, wavelength type, etc. Among them, phase type fiber optic acoustic sensors are developed based on different interference structures, including Michelson [5], [6], Fabry-Perot [3], [7], Mach-Zehnder [8], [9], and Sagnac structures [10], [11]. In contrast, acoustic sensors with F-P structure only require one fiber, forming an F-P cavity between the fiber end face and the vibrating diaphragm. The structure is simple, easy to miniaturize, and has high sensitivity, making it one of the current research highlights.

The F-P cavity is the core structure of extrinsic optical fiber microphone (OFM), usually composed of fiber end-face,

The associate editor coordinating the review of this manuscript and approving it for publication was S. M. Abdur Razzak.

cavity shell, and vibration diaphragm. Among them, the vibrating diaphragm is one of the main factors affecting the performance of the sensor, and the sensitivity of the diaphragm to external acoustic vibration directly affects the sensitivity of the sensor. Besides, the impact of preparation processes on the reliability and stability of the device cannot be ignored. Therefore, the appropriate membrane material and processing technology jointly determine the overall performance of the sensor. At present, various materials are utilized to prepare vibration membranes for F-P cavities, such as quartz [12], polymers [13], [14], [15], [16], (oxidized) graphene [17], [18], etc. Due to the high rigidity of quartz materials and their resistance to deformation, they are usually processed into temperature and strain sensors [13], [19]. Currently, polymer membranes are widely used in acoustic sensors. Although polymer membranes (such as PET, PP, etc.) are prone to deformation, their properties tend to decline after long-term use, such as hardening, embrittlement, loss of strength, etc. As one of the best comprehensive film materials at present, polyimide (PI) has extremely excellent electrical insulation, chemical/mechanical stability, aging resistance, and is a very promising engineering polymer [20], [21]. In addition, the reflectivity of polymer films is usually low, and a layer with high reflectivity such as Au, Ag, Al [22], [23], [24] needs to be coated on the fiber end-face or the surface of the polymer membrane. However, aluminum films are prone to oxidation and are not wear-resistant, and usually require a protective layer to be coated through complex and strict photolithography process [24]. Although silver film has high reflectivity in the visible light band, it inevitably reacts with sulfur-containing components in the atmosphere, resulting in a decrease in reflectivity and stability [1]. In contrast, gold film is not easily oxidized, which has superb stability and very high reflectivity in the air, making it an ideal candidate for reflecting layer.

In summary, we selected PI thin film as the substrate and adopted magnetron sputtering technology. A dense gold layer with a nanoscale thickness (about 400 nm) was deposited on the surface of polyimide (PI) film by physical vapor deposition (PVD), and a high-performance extrinsic F-P fiber optic microphone was obtained. Through adjustment and calculation, the optimal cavity length was found to be about 500 μm. In terms of sensitivity (170 mV/Pa), signal-to-noise ratio (72 dB @ 1 kHz) and other acoustic indicators, it is superior to the commercial electric microphone of Brüel & Kjær company. It has excellent response performance in the audio frequency range of 200-10 kHz and good linear sound pressure response, with a fitting coefficient of 0.9987. The material selection and process of this work have overcome the problems of insufficient material stability and insufficient process precision in existing work, and have excellent processability and repeatability. It is expected to achieve mass production, maintain performance stability in harsh environments, achieve high sensitivity sound pressure detection, and have broad application prospects.

II. THEORY

A. PRINCIPLE OF F-P OPTICAL FIBER MICROPHONE

To analyze the working principle of optical fiber microphone (OFM), firstly we focus on the vibrating diaphragm. As shown in Fig.1, if the external acoustic pressure acts uniformly on the surface of the diaphragm, it will cause deformation, which will convert the acoustic vibration into diaphragm vibration. When the deformation of the diaphragm center does not exceed 30% of its thickness, it could be assumed that there is a good linear relationship between the deformation of the diaphragm and the external acoustic pressure.

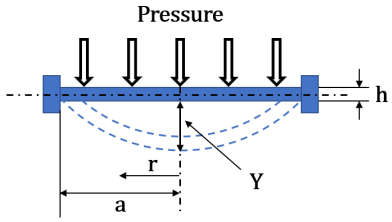

FIGURE 1. Schematic diagram of diaphragm deformation under uniform pressure.

According to theory [25], the deformation equation of the diaphragm under forced vibration could be derived as follows:

$$Y = \frac{3P\left(1-\mu\right)^2\left(\mathrm{a}^2-r^2\right)^2}{16Eh^3}\cdot\frac{f_{mn}^2}{\sqrt{\left(f_{mn}^2-f^2\right)^2+4f^2\xi^2}} \quad (1)$$

where Y represents the deformation variable at the center position of the diaphragm, P represents the sound pressure acting on the surface of the membrane, E, μ, h represent the Young's modulus, Poisson's ratio, and thickness of the film, a represents the radius of the diaphragm, and r represents the distance to the center of the diaphragm, ξ is the damping ratio, f is the frequency of the sound wave, f_{mn} is the mechanical resonance frequency, and its equation is:

$$f_{mn} = \frac{k_{mn}^2 h}{4\pi\,\mathrm{a}^2}\sqrt{\frac{E}{3\rho\left(1-\mu^2\right)}} \quad (2)$$

Among them, ρ is the mass density of the material, k_{mn} is a constant related to the order of mechanical resonance frequency. We could see from the above formula that for a given material, its properties such as E, μ and ρ are all fixed constants. It is obvious from Fig.2(a) that the deformation at the center of the diaphragm is the largest under uniform pressure. To make OFM sensitive, the diaphragm should generate as much deformation as possible, which requires increasing the radius or reducing its thickness. However, when the radius is too large or the thickness is too small, it could lead to a decrease in resonance frequency, thereby limiting the frequency range of flat response that OFM can produce. Therefore, determining the size of the diaphragm requires a comprehensive consideration of sensitivity and frequency response range, to obtain reasonable values in terms of radius and thickness.

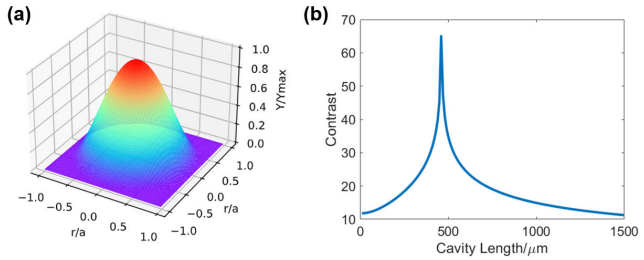

FIGURE 2. (a) The relationship between the deformation and the radial distance. (b) Simulation curves of interference fringe contrast varing with F-P cavity length.

We then divert attention to the F-P cavity structure consisting of two parallel reflection surfaces, that is, the fiber end-face and vibrating diaphragm. When light comes out of a source, part of it undergoes Fresnel reflection at the fiber end-face, while another portion undergoes transmission and continues propagating forward. When it reaches the Au/PI composite film, reflection occurs, coupling the light into the optical fiber. The deformation of the diaphragm causes a change in the F-P cavity length. To improve the performance of OFM, it is necessary to minimize the loss induced during optical transmission, as well as to select a specific cavity length to obtain the maximum interference contrast.

It is known that the following relationship [26] exists between the interference fringe contrast C and the loss coefficient K:

$$C = 20\log_{10}\left[\left|\frac{\sqrt{R_1} + K\left(1 - R_1\right)|n_x - n_m|/(n_x + n_m)}{\sqrt{R_1} - K\left(1 - R_1\right)|n_x - n_m|/(n_x + n_m)}\right|\right] \tag{3}$$

where n_x and n_m represent the refractive index of the sample and the medium, respectively. It could be seen that the value of K significantly affects the fringe contrast. To obtain high contrast interference fringes, it is necessary to minimize the transmission loss of light, and the addition of films with high reflectivity is a common and effective approach. The expression for the loss coefficient K could be written as:

$$K = \left(1 - A_1\right)\eta e^{-2\alpha L} \tag{4}$$

where A_1 is the transmission loss factor on the reflective surface R_1 caused by surface defects; α is the absorption coefficient of the optical medium in the cavity; and η represents the amplitude coupling efficiency, which is expressed as:

$$\eta = \left[1 + L^2\lambda^2/\left(\pi^2\omega_0^4\right)\right]^{-1/4} \tag{5}$$

where λ is the light wavelength and ω_0 is the beam waist of the optical fiber. By associating equation (3), (4) and (5), the equation for the interference fringe contrast C versus the cavity length L could be obtained. We assume the ideal case that there is no loss or absorption during optical transmission, and the simulation curve is obtained by plotting using MATLAB. As shown in Fig.2(b), the stripe contrast shows an increasing and then decreasing trend with the cavity length, and achieves a maximum value at a certain position. In fact, there must be loss and absorption of light by the medium and other circumstances. Despite the deviation of our values from the actual values, this does not affect the nature of the curve, that is, there is always a theoretical length of the cavity, so that the contrast of the stripe reaches an optimal value, and the specific value of the cavity length must be determined by experimental measurements.

B. DESIGN AND FABRICATION OF MEMBRANE-TYPE F-P FIBER OPTICAL MICROPHONE

The fabrication of the sensor involves the following steps:

(1) Obtain a metal sleeve with an inner diameter of 2.6 mm through mechanical processing as the housing for the sensor. After attempts, it has been found that this size of sleeve and film makes it easier to assemble and control costs.

(2) Use high-strength epoxy glue to fix the optical fiber ceramic core (inner diameter of 125 μm, outer diameter of 2.5 mm) to the metal sleeve, ensuring no relative sliding. Leave a certain distance at the top of the ceramic core and the metal sleeve to form an F-P cavity structure between the optical fiber end face and the vibrating membrane.

(3) Use a magnetron sputtering machine (PVD 75, LESKER) and gold target to prepare the Au/PI composite film. In this work, PI film is a commercially available product with a thickness of 15 μm (ρ = 1.38 g/cm^3). It should be noted that we also purchased PI films of 5 μm and 10 μm. However, it was found that these two films were poorly coated and prone to wrinkles and even delamination cracking, which did not occur with the 15 μm PI film. As for the selection of Au thickness, we mainly control the film thickness by holding the time of magnetron sputtering. To facilitate comparison, we set up three groups of 2 min, 5 min, and 8 min for coating at the suggestion of the PVD engineer. After evaluating the morphology and response properties of the composite film, we confirmed that the optimal coating time is 5 min and the thickness of the Au layer is about 400 nm.

(4) Use epoxy glue to affix the Au/PI membrane to the top of the metal sleeve. During this process, attention should be paid to keeping the membrane flat. Otherwise, the optical fiber end face and the membrane may not be parallel, leading to poor coupling of reflected light from the end-face and the inner surface of the membrane into the fiber for interference. Finally, use an optically adjustable support to align a single-mode fiber (G652B1) with a flat end-face to the ceramic core. Adjust the distance between the optical fiber end face and the inner surface of the vibrating membrane. Use an optical spectral analyzer (AQ6370D, Yokogawa) to observe the generated F-P interference spectrum and select an appropriate cavity length. The schematic diagram of the sensor structure and the actual object are shown in Fig.3.

Subsequently, an analysis of the F-P interference spectrum of the OFM was conducted. According to the free spectral range (FSR) of the sensing head [18], the F-P cavity length L was calculated by:

$$L = \frac{\lambda_1\lambda_2}{2\mathrm{n}\left(\lambda_1 - \lambda_2\right)} \tag{6}$$

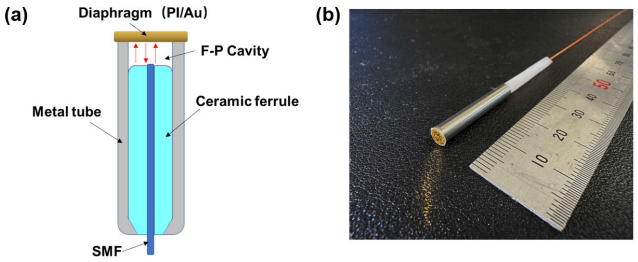

FIGURE 3. (a) Schematic diagram of the F-P acoustic sensor structure. (b) Actual image of the membrane-type F-P optical fiber microphone.

Here, λ_1 and λ_2 are the wavelengths corresponding to the two valleys (peaks) of the sensor interference spectrum near the center wavelength of the light source, and n is the refractive index of the F-P air cavity, typically taken as $n = 1$.

After fabrication, the cavity length was adjusted using a stepper motor (with a movement precision of up to micrometer level). The interference spectrum was then collected using the optical spectral analyzer, as shown in Fig.4. It is easy to notice that with the change of cavity length, the extinction ratio shows an increase and then decrease. The maximum extinction ratio is approximately 12 dB. Taking $\lambda_1 = 1550.24$ nm, and $\lambda_2 = 1547.84$ nm, the cavity length was calculated to be approximately 500 μm by using the peak-to-peak method.

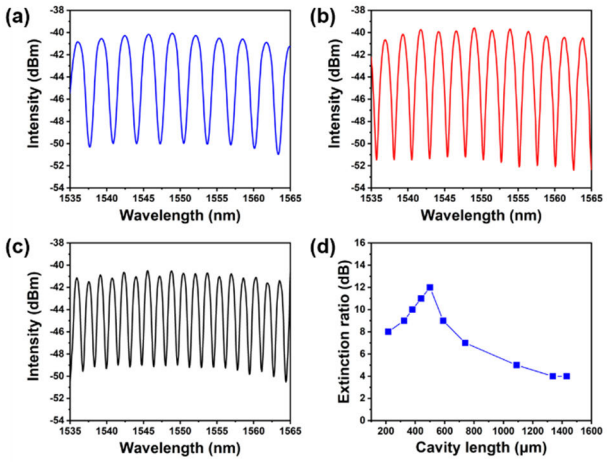

FIGURE 4. Interference spectra corresponding to OFMs with cavity lengths of (a) 380 μm, (b) 500 μm and (c) 740 μm. (d) Curve of extinction ratio with cavity length.

C. CHARACTERIZATION OF MATERIAL PROPERTIES OF AU/PI COMPOSITE FILM

We firstly characterized the morphology of Au/PI composite films using scanning electron microscopy (Gemini 500, Zeiss). From Fig.5, it could be observed that the surface of the composite film prepared by magnetron sputtering process is uniform and dense, and the thickness of PI is confirmed to be about 15 μm. The thickness of the Au layer on the upper surface is about 400 nm, and Au is tightly bound to PI without significant separation. This result proves the success of the PVD coating process.

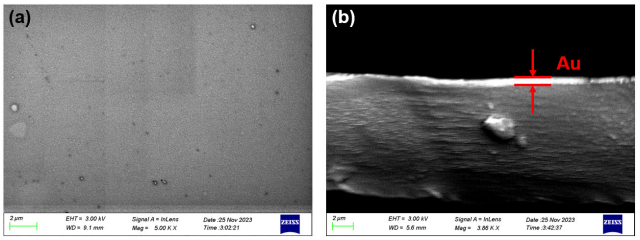

FIGURE 5. SEM images of the (a) gold-plated side surface and (b) cross-section of Au/PI composite films.

Secondly, we characterized the surface flatness of the composite film using a laser confocal microscope (inVia Qontor, Renishaw), and the results are shown in Fig.6. Adjust the magnification and focus on the analysis of an area measuring 1.3 mm × 1.3 mm, measurements were taken at two different cross-sections, and the results showed that the maximum surface roughness of the thin film was only 11 μm. Compared to similar reported work (Ag, 14 μm) [27], the improvement also indicates that the obtained film has good flatness and highlights the excellent process precision of PVD method, which is conducive to the large-scale preparation of devices.

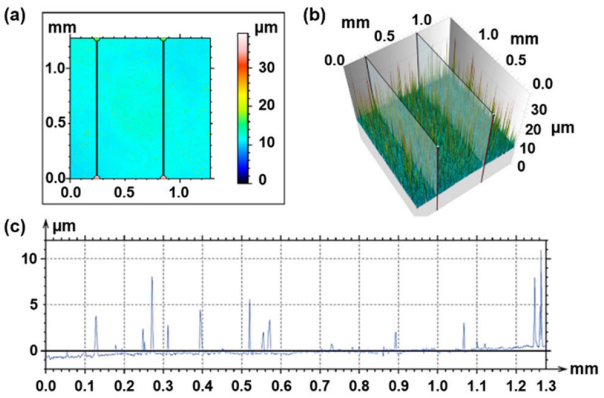

FIGURE 6. (a) Scanning image of surface flatness of the film. (b) Schematic diagram for testing the flatness of different cross-sections of the film. (c) The flatness result curve of the film at different cross-sections.

Subsequently, to demonstrate the superiority of using Au as a high reflection coating, we tested the reflectivity of composite films with sputtered Au and Ag coatings, as well as PI films without sputtering, in the visible and near-infrared bands. The test used a planar array backlight spectrometer (PG2000 Pro, ideaopics) and a near-infrared spectrometer (NIR25S, ideaopics), with an aluminum mirror as the reference.

As shown in Fig.7, the reflectivity of the composite film after sputtering the metal coating is generally higher than that of a single PI film in the visible/invisible light band range; Among them, the reflectivity of Au is still higher than that of Ag coating in the full wavelength range, and its stability is also better than that of Ag. Due to the use of a semiconductor laser with a central wavelength of 1550 nm in this work, it is more reasonable to choose Au as the coating. In brief, we have successfully prepared highly reflecting layer on the surface of

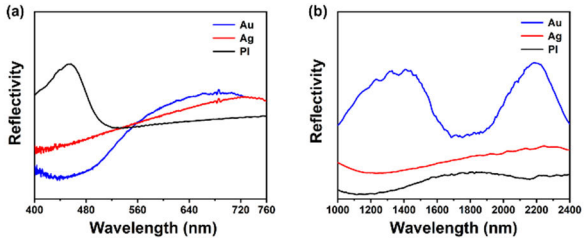

FIGURE 7. (a) Reflectance curves of Au, Ag, and PI in the visible light band. (b) Reflectance curves of Au, Ag, and PI in the invisible light band.

commercial PI film by sputtering Au using PVD technology. Multiple characterization results show that the morphology and bonding of the composite film are exceptional, with significant improvements in parameters such as flatness and reflectivity compared to previous work. After adjustment and calculation, the optimal cavity length was determined to be 500 μm, which lays the foundation for the excellent acoustic performances of the sensor.

III. EXPERIMENT

A. SETUP OF THE ACOUSTIC TESTING SYSTEM

We selected the B&K 4939 electric microphone from the Danish company Brüel & Kjær as a reference group for subsequent experiments.

The self-built testing system, as shown in Fig.8, positions the self-made OFM and the reference B&K 4939 on either side of the sound source symmetrically, ensuring that both receive identical acoustic signals. Moreover, a standard signal generator is used to control the frequency and sound pressure of the sound source.

The output signal from the B&K 4939, after processing through a preamplifier system (B&K 2690), yields the frequency and amplitude of the incident sound pressure.

The light source used is the 1550.12 nm single-frequency narrowband laser (BASIK X15, NKT Photonics). The signals from the two microphones are processed and analyzed through a computer program after passing through a digital acquisition card (USB-4431, NI).

B. FREQUENCY RESPONSE TEST

Frequency response is an important metric for evaluating microphone performance. We tested the microphone's frequency response performance in the 50-20 kHz range. During testing, a signal generator is used to play sine wave sound signals, and a standard sound pressure meter is used to read the sound pressure intensity. The sound pressure is kept constant, and only the frequency of each signal is changed. Sinusoidal sound waves with frequencies ranging from 100 Hz to 20 kHz are played sequentially in steps of 100 Hz. The corresponding output results are collected each time, and the frequency response curve is plotted as shown in Fig.9.

According to Fig.9, it could be seen that OFM has a basically flat response curve in the range of 200-10 kHz. The curve of the B&K 4939 is relatively flatter when evaluated over the entire frequency range. On the other hand, if one

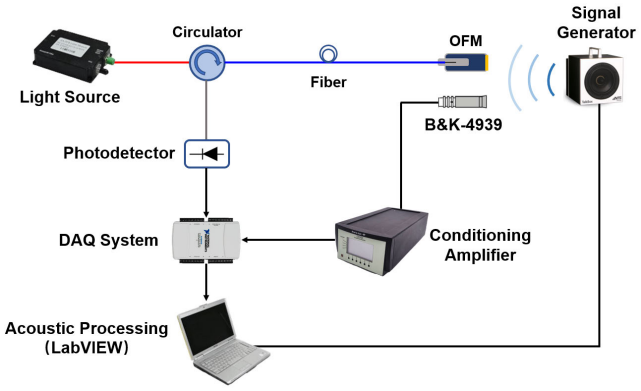

FIGURE 8. Schematic diagram of the experimental system for measuring the acoustic properties of OFM and B&K 4939.

focuses on the intensity of the signal output, it becomes clear that self-made OFM almost always produces a clearer output for inputs with the same sound pressure but different frequencies. Furthermore, it should be noted that the frequency response curve of OFM exhibits a maximum at approximately 14 kHz, which can be considered to correspond to the fundamental mechanical resonance frequency of the Au/PI vibrating diaphragm. Similarly, Li et al. [24] reported a sound sensor developed using Al/PI film with a mechanical resonance frequency of approximately 9 kHz, while our Au/PI composite film has a larger resonance frequency and a wider response range, making it more practical in comparison.

C. SENSITIVITY AND SNR TEST

When testing sensitivity, firstly use a standard sound pressure gauge to read the sound pressure intensity of the input signal. Secondly, place the standard sound pressure gauge and the sound source on the same horizontal line, play a sine wave sound signal with a frequency of 1000 Hz, and adjust the distance between the sound pressure gauge and the sound source so that the sound pressure level received by the sound pressure gauge is 94 dB SPL (equivalent to a sound pressure value of 1 Pa). Subsequently, replace the position of the sound pressure gauge with a microphone, and the value of the output voltage is the sensitivity of the microphone.

To further illustrate the effect of Au layer on the surface of the PI film on the performance of OFM, we tested OFMs based on Au/PI composite film and single PI film. We then put the two OFMs with B&K 4939 under same conditions. As shown in Fig.10, the output voltage amplitudes of OFM based on Au/PI composite film, OFM based on single PI film and B&K 4939 were measured to be 0.170 V, 0.012 V, and 0.004 V, respectively, at 94 dB SPL/1000 Hz sinusoidal signals. Therefore, the sensitivities of the two OFMs were 170 mV/Pa and 12 mV/Pa, while that of B&K 4939 is 4 mV/Pa, which is very close to the reference value in the product manual (4.38 mV/Pa). At this point, the power spectral density after Fast Fourier Transform (FFT) is shown in Fig.11. According to the calculation, the SNR of the OFM based on the Au/PI composite film is about 76 dB, which is

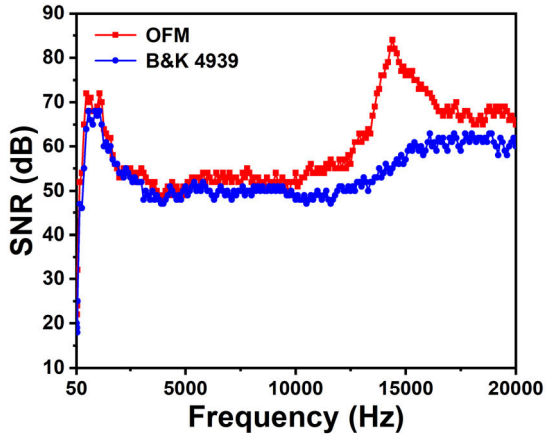

FIGURE 9. Frequency response curves of OFM and B&K 4939 in the range of 50-20 kHz.

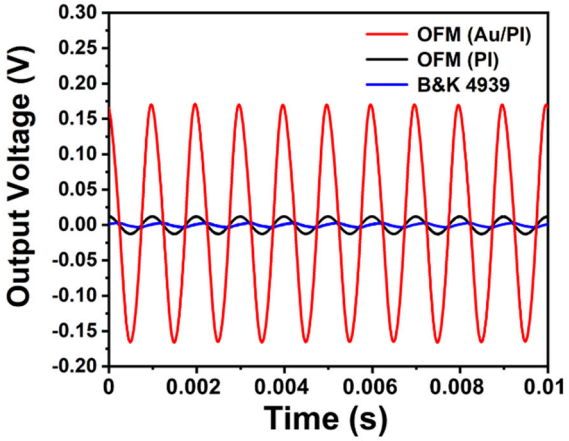

FIGURE 10. Output response curves of OFM based on Au/PI composite film, OFM based on single PI film and B&K 4939 under test conditions of 1000 Hz/94 dB SPL.

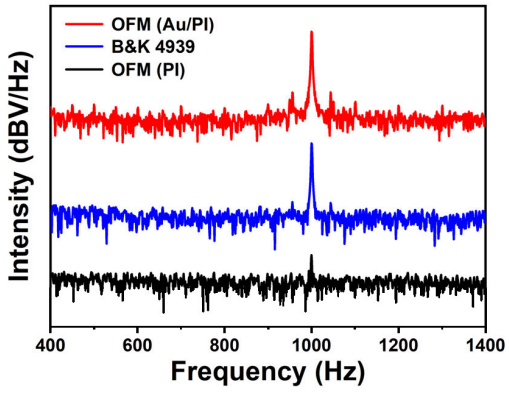

FIGURE 11. SNR test results of OFM based on Au/PI composite film, OFM based on single PI film and B&K 4939 at 1000 Hz.

also higher than that of the B&K 4939 (62 dB) and that of the OFM based on single PI film (21 dB). This shows that adding Au layer on the surface of PI film has a significant effect on the sensitivity and SNR of the OFM. Therefore, it is more reasonable to choose the Au/PI composite film rather than a single PI film as the vibrating film for the F-P cavity.

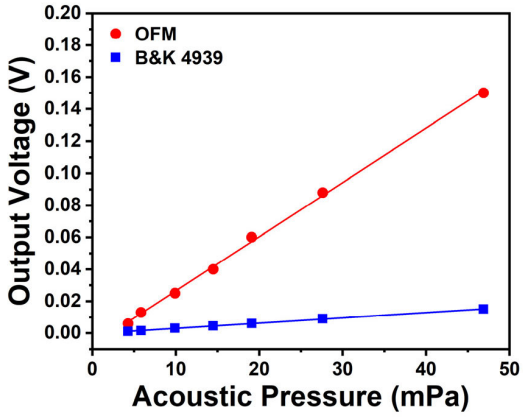

FIGURE 12. Output voltage signals of OFM and B&K 4939 for varying applied acoustic pressure levels at the frequency of 1000 Hz.

D. LINEARITY TEST (PRESSURE-OUTPUT VOLTAGE LINEAR VARIATION)

During testing, we selected a 1000 Hz sine wave signal as input, kept the frequency of the signal constant, and continuously increased the sound pressure level intensity of the signal. We recorded the value of the sound pressure intensity of each test input signal and the output voltage, plotted it as a scatter plot, and then performed linear fitting.

It can be observed in Fig.12 that within the range of 0-50 mPa acoustic pressure variation, the output response of the two microphones shows a good linear relationship with the sound pressure variation, with fitting coefficients of 0.9987 and 0.9993, respectively. In addition, the slope of the fitting curve of OFM is higher than that of B&K 4939, indicating that under the same sound pressure changes, the output response of OFM is higher than that of B&K 4939.

We characterized and tested the new diaphragm type F-P fiber optic microphone reported in this paper from material properties and acoustic measurements, and conducted preliminary research and revelation on its structure-efficiency relationship. By comparing with a commercial electrical microphone, the advantages of OFM in certain acoustic parameters are demonstrated. However, currently it is still a long-term and arduous journey before the OFM becomes a mature product like Optimic 1140. For instance, the size ratio (radius, thickness, etc.) of PI and Au film, and the process parameters of magnetron sputtering could be further optimized; In terms of system construction and device packaging, lower phase noise light sources and low thermal noise optoelectronic devices can also be used, and anti-interference nets can be installed on the sensing head to further enhance the overall stability and performance of OFM.

IV. CONCLUSION

In summary, this article reports a novel extrinsic Fabry-Perot fiber optic acoustic sensor based on Au/PI composite film. The film prepared by PVD process has high reflectivity and excellent flatness, and a high-performance OFM with a F-P cavity length of 500 μm has been successfully fabricated. Under testing condition of 1000 Hz/94dB, the sensitivity is

about 170 mV/Pa, which is much higher than the commercial electric microphone B&K 4939. The maximum SNR can reach 76 dB. In addition, the OFM also has good frequency response performance in the range of 200-10 kHz, and there is a good linear relationship between the output voltage of OFM and the input sound pressure, with a fitting coefficient of 0.9987. From a certain point of view, the material selection and process of this work have overcome the limitations of previous materials and technique, and possess superb processability and repeatability. It is expected to achieve high sensitivity acoustic detection within audible range in harsh environments (such as electromagnetic interference, extreme temperature/humidity, etc.)

REFERENCES

[1] B. Liu, H. Zhou, L. Liu, X. Wang, M. Shan, P. Jin, and Z. Zhong, "An optical fiber Fabry–Pérot microphone based on corrugated silver diaphragm," *IEEE Trans. Instrum. Meas.*, vol. 67, no. 8, pp. 1994–2000, Aug. 2018.

[2] K. Chen, "Fast demodulated white-light interferometry-based fiber-optic Fabry–Pérot cantilever microphone," *Opt. Lett.*, vol. 43, no. 14, pp. 3417–3420, Jul. 2018.

[3] X. Lu, Y. Wu, Y. Gong, and Y. Rao, "A miniature fiber-optic microphone based on an annular corrugated MEMS diaphragm," *J. Lightw. Technol.*, vol. 36, no. 22, pp. 5224–5229, Nov. 2018.

[4] M. Islam, M. Ali, M.-H. Lai, K.-S. Lim, and H. Ahmad, "Chronology of Fabry–Pérot interferometer fiber-optic sensors and their applications: A review," *Sensors*, vol. 14, no. 4, pp. 7451–7488, Apr. 2014.

[5] L. Liu, P. Lu, H. Liao, S. Wang, W. Yang, D. Liu, and J. Zhang, "Fiber-optic Michelson interferometric acoustic sensor based on a PP/PET diaphragm," *IEEE Sensors J.*, vol. 16, no. 9, pp. 3054–3058, May 2016.

[6] T. Jiang, D. Ba, and Y. Dong, "Online distributed strain measurement of fiber Michelson hydrophones based on DPP-BOTDA with a pulsed-probe wave," *Opt. Exp.*, vol. 27, no. 16, p. 22375, 2019.

[7] L. Liu, P. Lu, S. Wang, X. Fu, Y. Sun, D. Liu, J. Zhang, H. Xu, and Q. Yao, "UV adhesive diaphragm-based FPI sensor for very-low-frequency acoustic sensing," *IEEE Photon. J.*, vol. 8, no. 1, pp. 1–9, Feb. 2016.

[8] E. I. Pacheco-Chacon, J. M. Sierra-Hernandez, E. Gallegos-Arellano, M. S. Avila-Garcia, M. Bianchetti, I. Hernandez-Romano, Y. Lopez-Dieguez, L. A. Herrera-Piad, and R. Rojas-Laguna, "An aluminum-coated asymmetric core-offset Mach–Zehnder interferometer temperature sensor," *Opt. Fiber Technol.*, vol. 65, Sep. 2021, Art. no. 102591.

[9] J. Geng and N. Kishi, "A simultaneous audio and temperature sensing system based on in-line Mach–Zehnder interferometer," *Opt. Fiber Technol.*, vol. 81, Dec. 2023, Art. no. 103524.

[10] Z. Cheng, J. Zeng, D. Liang, C. Chang, and B. Wang, "Influence of initial phase modulation on the sensitivity of the optical fiber Sagnac acoustic emission sensor," *Appl. Sci.*, vol. 9, no. 5, p. 1018, Mar. 2019.

[11] A. A. Zhirnov, T. V. Choban, K. V. Stepanov, K. I. Koshelev, A. O. Chernutsky, A. B. Pnev, and V. E. Karasik, "Distributed acoustic sensor using a double Sagnac interferometer based on wavelength division multiplexing," *Sensors*, vol. 22, no. 7, p. 2772, Apr. 2022.

[12] T. Liu, J. Yin, J. Jiang, K. Liu, S. Wang, and S. Zou, "Differential-pressure-based fiber-optic temperature sensor using Fabry–Pérot interferometry," *Opt. Lett.*, vol. 40, no. 6, pp. 1049–1052, Mar. 2015.

[13] M. S. Ferreira, P. Roriz, J. Bierlich, J. Kobelke, K. Wondraczek, C. Aichele, K. Schuster, J. L. Santos, and O. Frazão, "Fabry–Pérot cavity based on silica tube for strain sensing at high temperatures," *Opt. Exp.*, vol. 23, no. 12, p. 16063, Jun. 2015.

[14] Y. Zhao, M.-Q. Chen, F. Xia, and R.-Q. Lv, "Small in-fiber Fabry–Pérot low-frequency acoustic pressure sensor with PDMS diaphragm embedded in hollow-core fiber," *Sens. Actuators A, Phys.*, vol. 270, pp. 162–169, Feb. 2018.

[15] B. Liu, X. Zhang, A. Wang, Y. Liu, Y. Wang, M. Shan, L. Liu, P. Jin, and Z. Zhong, "Optical fiber Fabry–Pérot acoustic sensors based on corrugated PET diaphragms," *IEEE Sensors J.*, vol. 21, no. 13, pp. 14860–14867, Jul. 2021.

[16] S. E. Hayber, T. E. Tabaru, S. Keser, and O. G. Saracoglu, "A simple, high sensitive fiber optic microphone based on cellulose triacetate diaphragm," *J. Lightw. Technol.*, vol. 36, no. 23, pp. 5650–5655, Dec. 2018.

[17] J. Ma, H. Xuan, H. L. Ho, W. Jin, Y. Yang, and S. Fan, "Fiber-optic Fabry–Pérot acoustic sensor with multilayer graphene diaphragm," *IEEE Photon. Technol. Lett.*, vol. 25, no. 10, pp. 932–935, May 2013.

[18] Y. Wu, C. Yu, F. Wu, C. Li, J. Zhou, Y. Gong, Y. Rao, and Y. Chen, "A highly sensitive fiber-optic microphone based on graphene oxide membrane," *J. Lightw. Technol.*, vol. 35, no. 19, pp. 4344–4349, Oct. 2017.

[19] S. Liu, "High-sensitivity strain sensor based on in-fiber improved Fabry–Pérot interferometer," *Opt. Lett.*, vol. 39, no. 7, pp. 2121–2124, Apr. 2014.

[20] D.-J. Liaw, K.-L. Wang, Y.-C. Huang, K.-R. Lee, J.-Y. Lai, and C.-S. Ha, "Advanced polyimide materials: Syntheses, physical properties and applications," *Prog. Polym. Sci.*, vol. 37, no. 7, pp. 907–974, Jul. 2012.

[21] M. Zhang, L. Wang, H. Xu, Y. Song, and X. He, "Polyimides as promising materials for lithium-ion batteries: A review," *Nano-Micro Lett.*, vol. 15, no. 1, p. 135, Dec. 2023.

[22] Z. Xiang, W. Dai, W. Rao, X. Cai, and H. Fu, "A gold diaphragm-based Fabry–Pérot interferometer with a fiber-optic collimator for acoustic sensing," *IEEE Sensors J.*, vol. 21, no. 16, pp. 17882–17888, Aug. 2021.

[23] F. Xu, J. Shi, K. Gong, H. Li, R. Hui, and B. Yu, "Fiber-optic acoustic pressure sensor based on large-area nanolayer silver diaghragm," *Opt. Lett.*, vol. 39, no. 10, p. 2838, 2014.

[24] X. Li, S. Zhen, K. Qian, X. Liang, X. Wang, J. Shi, X. Wu, and B. Yu, "A heat-resistance and high-sensitivity acoustic pressure sensor based on aluminum-polyimide diaphragm," *Sens. Actuators A, Phys.*, vol. 279, pp. 75–78, Aug. 2018.

[25] W. Ni, P. Lu, X. Fu, W. Zhang, P. P. Shum, H. Sun, C. Yang, D. Liu, and J. Zhang, "Ultrathin graphene diaphragm-based extrinsic Fabry–Pérot interferometer for ultra-wideband fiber optic acoustic sensing," *Opt. Exp.*, vol. 26, no. 16, p. 20758, 2018.

[26] Y. Huang, J. Tao, and X. Huang, "Research progress on F-P interference—Based fiber-optic sensors," *Sensors*, vol. 16, no. 9, p. 1424, Sep. 2016.

[27] B. Liu, J. Lin, H. Liu, A. Jin, and P. Jin, "Extrinsic Fabry–Pérot fiber acoustic pressure sensor based on large-area silver diaphragm," *Microelectronic Eng.*, vol. 166, pp. 50–54, Dec. 2016.

ZEKUN ZHU received the B.S. degree from Donghua University, in 2019, where he is currently pursuing the M.S. degree with Fudan University. His current research interests include optical fiber sensing and technology.

HANYU SHUAI received the B.S. degree from Fudan University, in 2022, where she is currently pursuing the M.S. degree. Her current research interests include optical fiber sensing and applications.

KUN JIA received the B.S. degree from Fudan University, in 2020, where he is currently pursuing the Ph.D. degree. His current research interests include optical interferometer and optical sensing.

YUANYUAN SUN received the B.S. degree from Fudan University, in 2021, where she is currently pursuing the M.S. degree. Her current research interests include optical fiber sensing and energy transfer application.

BO JIA received the Ph.D. degree from the University of Electronic Science and Technology of China, in 2000. He is currently a Professor with the Department of Material Science, Fudan University, Shanghai. His research interests include fiber-optic sensor and applications, and optical communication.

PENGWEI ZHOU received the B.S. degree from China University of Petroleum, Shandong, in 2013, and the Ph.D. degree from Fudan University, Shanghai, China, in 2018. From 2018 to 2022, he was a Post-Doctoral Fellow. Since 2022, he has been an Associate Professor with Fudan University. His research interest includes fiber optic communication and sensing.